

Blood-brain barrier leakage is increased in Parkinson's disease

Sarah Al-Bachari^{1,2,3}, Josephine H Naish^{5,6}, Geoff JM Parker^{6,7}, Hedley CA Emsley^{1,2,3}, Laura M Parkes^{3,4}

^{1.} Lancaster Medical School, Lancaster University, UK;

^{2.} Department of Neurology, Lancashire Teaching Hospitals NHS Foundation Trust, Preston, UK;

^{3.} Division of Neuroscience and Experimental Psychology, Faculty of Biology, Medicine and Health, The University of Manchester, Manchester, UK;

^{4.} Geoffrey Jefferson Brain Research Centre, Manchester Academic Health Science Centre, Manchester, UK;

^{5.} Division of Cardiovascular sciences, Faculty of Biology, Medicine and Health, University of Manchester, UK;

^{6.} Bioxydyn Limited, Manchester, UK;

^{7.} Centre for Medical Image Computing, Department of Computer Science and Department of Neuroinflammation, University College London, United Kingdom.

Correspondence:

Dr Laura M Parkes

Address: Zochonis Building, University of Manchester, Manchester, M13 9PL.

Email: Laura.Parkes@manchester.ac.uk

Keywords: Blood-brain barrier, cerebrovascular disease, dynamic contrast enhanced MRI, Parkinson's disease, neurovascular

Number of Words: 4500

Number of Figures: 4

Number of Tables: 2

Language: British English

Background: Blood-brain barrier disruption has been noted in animal models of Parkinson's disease (PD) and forms the basis of the vascular hypothesis of neurodegeneration, yet clinical studies are lacking.

Objective: To determine alterations in blood-brain barrier integrity in PD, with comparison to cerebrovascular disease.

Methods: Dynamic contrast enhanced magnetic resonance images were collected from 49 PD patients, 15 control subjects with cerebrovascular disease (control positive CP) and 31 healthy control subjects (control negative CN), with all groups matched for age. Quantitative maps of the contrast-agent transfer coefficient across the blood-brain barrier (K^{trans}) and plasma volume (v_p) were produced using Patlak analysis. Differences in K^{trans} and v_p were assessed with voxel-based analysis as well as in regions associated with PD pathophysiology. In addition, the volume of white matter lesions (WML) was obtained from T₂-weighted fluid attenuation inversion recovery (FLAIR) images.

Results: Higher K^{trans} , reflecting higher blood-brain barrier leakage, was found in the PD group than in the CN group using voxel-based analysis; differences were most prominent in the posterior white matter regions. Region of interest analysis confirmed K^{trans} to be significantly higher in PD than in CN, predominantly driven by differences in the substantia nigra, normal-appearing white matter, WML and the posterior cortex. WML volume was significantly higher in PD compared to CN. K^{trans} values and white matter lesion volume were similar in PD and CP, suggesting a similar burden of cerebrovascular disease despite lower cardiovascular risk factors.

Conclusion: These results show blood-brain barrier disruption in PD.

Abbreviations:

ANOVA – analysis of variance, BBB – blood-brain barrier, CA – caudate, CN – control negative, CP – control positive, CSF – cerebral spinal fluid, DCE-MRI – dynamic contrast enhanced magnetic resonance imaging, FLAIR – fluid attenuation inversion recovery, FC – frontal cortex, FWE – family wise error, Hct – haematocrit, K^{trans} – contrast agent endothelial transfer coefficient, LEDD – Levodopa equivalent daily dose, MNI – Montreal Neurological Institute, MoCA – Montreal cognitive assessment, NAWM – normal appearing white matter, NHS – National Health Service, P – pallidum, PET – positron emission tomography, PC – posterior cortices, PD – Parkinson's disease, PU – putamen, ROI – region of interest, SN – substantia nigra, SNpc – substantia nigra pars compacta, SPM – statistical parametric mapping, T₁-FFE – T₁ fast field echo, TE – echo time, 3 T – 3 tesla, TR – repetition time, UPDRS – Unified Parkinson's Disease Rating Scale, v_p – plasma volume, VEGF – vascular endothelial growth factor, WML – white matter lesion.

1 Introduction

The blood-brain barrier (BBB) consists of highly specialised, metabolically active cells forming a selectively permeable, highly resistant barrier to diffusion of blood products (1). It is closely coupled with glial cells (i.e. pericytes, microglia, oligodendroglia, and astrocyte end-feet), all in close proximity to a neuron; collectively termed the neurovascular unit (2, 3). Normal functioning of the neurovascular unit ensures healthy function of the BBB and adequate cerebral blood flow, it also maintains the neuronal 'milieu' which is required for proper functioning of neuronal circuits and ensures the metabolic needs of the neurons are met (4, 5). In the neurovascular unit, BBB permeability and cerebral blood flow are mainly controlled by endothelial cells, smooth muscle cells and pericytes; damage to which have been associated with accumulation of neurotoxins and hypoxia leading to neuronal injury and loss (6, 7).

Neurodegeneration is now understood to be the consequence of multiple factors acting and interacting over time to lead to neuronal dysfunction and death (8-10). Neurovascular unit dysfunction, unsurprisingly, contributes to neuronal dysfunction and death; this forms the basis of the 'vascular model of neurodegeneration' (4, 11-15). The two pillars of this model are hypoperfusion and BBB disruption, both contributing to the vicious circle of neuronal loss. Studies particularly in the preclinical setting, suggest microvascular pathology and hypoperfusion occurs in the context of neurodegenerative diseases (4, 16-19). In addition studies in Parkinson's disease (PD) have revealed vascular remodeling, altered vasculature and abnormal angiogenesis (20-26).

Understanding of the pathogenesis of PD centres around the selective and progressive loss of dopaminergic neurons in the substantia nigra pars compacta (SNpc) and its connections with other basal ganglia structures. BBB disruption contributing to neurodegeneration in the SNpc has been reported in PD in animal studies (26-28). In humans, a relatively small PET study in PD patients revealed dysfunction of the BBB transporter system (29). A histological study revealed significantly increased permeability of the BBB in the post commissural putamen of PD patients (30). Thus the areas implicated in PD pathology have been shown to demonstrate BBB disruption, yet studies remain few and predominantly in animal models.

Many studies describe hypoperfusion in the posterior cortices in PD, in particular in the posterior parieto-occipital cortex, precuneus and cuneus and temporal regions with variable patterns in the frontal lobe (31-35). The extent to which BBB disruption impacts perfusion and vice versa (hypoperfusion influencing BBB disruption) is poorly understood. However, both occur at the microvascular level and may be linked. If this is the case, this then suggests that alterations in BBB may also be expected in these posterior regions as well as in regions implicated in PD pathology such as the basal ganglia, where neuronal loss and loss of nigrostriatal projections occurs.

Advances in neuroimaging techniques, in particular quantitative MRI techniques such as arterial spin labelling and dynamic contrast enhanced MRI (DCE-MRI), have paved the way for studies of the microcirculation in the clinical setting, with DCE-MRI specifically probing BBB integrity (36). Previously applied to measure BBB disruption in tumours, multiple sclerosis and acute ischemic stroke, recent applications have used this technique to probe more subtle and chronic BBB disruption. Studies include small vessel disease (37), Alzheimer's disease (38), mild cognitive impairment and normal ageing (39), vascular cognitive impairment (40) and diabetes (41) ; its value in these settings has been systematically reviewed (42). To our knowledge there is no published work on DCE-MRI measures in PD.

We used DCE-MRI to investigate regional alterations in BBB permeability in the context of PD. PD was compared with a control group with known cerebrovascular disease (control positive (CP)) and a control group without known cerebrovascular disease or PD (control negative (CN)). Our aim was to investigate whether potential changes are simply attributable to co-existing cerebrovascular disease in an aging population or if a pattern of BBB alterations specific to PD is revealed. Inclusion of the CP group allows us to do this by comparing the pattern of BBB disruption in the PD and CP groups with reference to the burden of cerebrovascular disease in each group, defined by white matter lesion (WML) volume as an accepted surrogate marker of small vessel disease. We hypothesized that BBB disruption in PD would occur in the basal ganglia structures due to the pathophysiology of PD being centred around selective and progressive loss of dopaminergic neurons in the SNpc and nigrostriatal pathways. Therefore, based on the vascular hypothesis of neurodegeneration, these areas should display BBB disruption. We also expected BBB disruption to occur in posterior and frontal cortices given that hypoperfusion, which potentially impacts BBB function, has been noted in these regions in PD. Finally, as BBB alterations in cerebrovascular disease have been found within WML and in the normal-appearing white matter (NAWM) (43) we also considered alterations in these regions. Hence we investigated BBB changes in basal ganglia, posterior and frontal cortex regions, NAWM and WML, along with a more exploratory voxel-wise analysis across the entire brain.

2. Materials and Methods

2.1 Approvals, recruitment, eligibility and consent

Relevant approvals were obtained including NHS ethical approval (North West – Preston Research Ethics Committee), research governance and local university approvals. PD patients were recruited from Lancashire Teaching Hospitals NHS Foundation Trust and Salford Royal NHS Foundation Trust. Eligibility criteria for PD participants were a clinical diagnosis of PD fulfilling UK Parkinson's disease society brain bank criteria (www.ncbi.nlm.nih.gov/projects) without known clinical cerebrovascular disease (no history of transient ischaemic attack or stroke) or dementia (44). Participants with cerebrovascular disease were recruited from patients attending Lancashire Teaching Hospitals with a clinical diagnosis of stroke or transient ischaemic attack within the previous 2 years (and at least 3 months prior to participation) supported by relevant brain imaging (control positives, CP). Controls without a history of either PD or clinical cerebrovascular disease were also recruited from the local community (control negatives, CN). All groups were matched for age. All participants were required to provide written informed consent and had capacity to do so.

2.2 Clinical assessments

PD assessment included the Unified Parkinson's Disease Rating Scale (UPDRS) (www.mdvu.org/library/ratingscales/pd/updrs.pdf) during the scan visit. Disease severity was measured using the Hoehn and Yahr rating scale (45). No alterations were made to the participants' medications for the study protocol. Routine clinical baseline data were also recorded and the levodopa equivalent daily dose (LEDD) calculated (46). A battery of clinical scales was also administered, including the Montreal Cognitive Assessment (MoCA) (www.MoCAtest.org) to measure cognition. Demographics and clinical data were compared between PD and control participants using unpaired Student's t-test for continuous variables or Fisher's exact test for categorical variables with p-value set at < 0.05.

146 2.3 MRI protocol

147 Participants were scanned on one of two systems running the same software version: a 3.0 T Philips
 148 Achieva scanner with an 8 channel head coil at Salford Royal Hospital or a separate 3.0 T Philips
 149 Achieva scanner with a 32 channel head coil at the Manchester Clinical Research Facility.
 150 Involuntary movements in participants were minimised using padding within the head coil.

151 Both scanners ran an identical MRI protocol. A DCE-MRI dynamic series of 160 3D T₁-weighted
 152 images (T₁ Fast Field Echo; T₁-FFE) were acquired with a temporal resolution of 7.6 seconds, spatial
 153 resolution of 1.5 x 1.5 x 4 mm, and total duration of approximately 20 minutes. On the 8th dynamic,
 154 a gadolinium-based contrast agent (Dotarem) bolus was administered using a power injector. The
 155 volume administered was proportional to the weight of the subject with a dose of 0.1 mmol/kg.

156 Prior to the dynamic scan, a series of additional 3D T₁-FFE images were acquired at 3 flip angles (2,
 157 5 and 10 degrees) in order to calculate a pre-contrast T₁ map using the variable flip angle method. A
 158 B₁ map was also collected in order to correct for B₁ field inhomogeneities.

159 In addition, a 1 mm isotropic 3D T₁-weighted image and a T₂-weighted FLAIR image were acquired.
 160 Please see supplementary material for full details of acquisition parameters.

161 2.4 MRI analysis

162 2.4.1 White matter lesion volume estimation

163 WML volume was calculated as an established marker of small vessel disease (47). WML volume
 164 was estimated using the lesion segmentation toolbox (48) in SPM8 using both T₂-weighted FLAIR
 165 images and T₁-weighted images as inputs. A threshold of 0.3 was chosen as it gave the most accurate
 166 estimates in a sub-study comparing WML volume estimates from the lesion segmentation toolbox
 167 with those from semi-automated lesion-growing methods on a subset of the data (n = 51, including
 168 representation from all groups, unpublished) (<https://www.statistical-modelling.de/1st.html>). WML
 169 volumes were positively skewed and were therefore cube-root transformed as is commonly done (49)
 170 before group comparisons using un-paired t-tests.

172 2.4.2 DCE analysis

173 The dynamic series of 160 images were first corrected for motion using the 'realignment' option in
 174 SPM12 (www.fil.ion.ucl.ac.uk/spm), which aligned all DCE-MRI images to the first image in the
 175 time-series. A vascular input function was derived from the sagittal sinus (50), which was delineated
 176 using MRIcro on the final image of the motion-corrected dynamic time series. Regions of
 177 approximately 50 voxels were selected. A voxel-by-voxel fit of the dynamic data for both the
 178 contrast agent transfer coefficient (K^{trans}) and plasma volume (v_p) was performed using the uptake or
 179 'Patlak' model assuming unidirectional transport of the tracer from the blood plasma to the
 180 extravascular, extracellular space. Further details regarding DCE-MRI analysis can be found in
 181 Supplementary Material.

182 Mean images of K^{trans} and v_p in each of the three groups were created following spatial smoothing
 183 using a 3D 3 mm full-width-half-maximum kernel in and visually inspected for differences. Voxel-
 184 wise analysis was performed using the SPM12 PET toolbox to determine regional differences in K^{trans}
 185 and v_p between the groups. K^{trans} and v_p maps were co-registered to the high resolution 3D T₁-

weighted image and then normalized to Montreal Neurological Institute (MNI) space. The normalised K^{trans} and v_p maps were spatially smoothed using an 8 mm full-width-half-maximum kernel. Voxel-wise comparisons of K^{trans} and v_p between the groups were performed, without intensity normalisation, using a two-sample unpaired t-test (unequal variances). Group comparisons were performed between: CN and PD, CP and PD and CP and CN. Regions were considered to show significant group differences at a voxel-level threshold of $p < 0.001$ uncorrected, and a minimum cluster size of 50 voxels, masked to the intra-cranial volume. Further analysis using family-wise error (FWE) correction for multiple comparisons at the cluster level was performed. The MNI coordinates were used to identify regions showing group differences using xjview V 8.14 (<http://www.alivelearn.net/xjview8/>).

Group differences in K^{trans} and v_p were also assessed in regions of interest (ROI) including the basal ganglia, frontal and posterior cortices, WML and NAWM. WML regions were obtained using the co-registered binary lesion masks from the lesion segmentation (see section 2.4.1) and care was taken to remove regions of WML from all other ROIs. The caudate (CA), putamen (PU) and pallidum (P) regions were obtained from MNI atlases (51, 52). The substantia nigra (SN) region was manually drawn on the T₂-weighted template image from SPM by an experienced researcher. Frontal and selected posterior cortical regions were also defined (in keeping with regions of hypoperfusion in other studies) (30, 33, 34, 53) using a combination of regions from the automatic anatomical labelling atlas (51). The frontal region consisted of superior and middle frontal gyri and the posterior region of precuneus, cuneus, lingual, superior and middle occipital gyri. Finally, NAWM was also selected, defined using the mask from the segmentation of the co-registered T₁-weighted image, in order to determine the significance of any diffuse differences between the groups. Figure 1 depicts the location of these ROIs. Mean K^{trans} and v_p values were extracted from each of these regions for each subject. Repeated measures ANOVA was performed with factors 'group' and 'region' to determine any significant difference in K^{trans} and v_p between the groups with 'subject' included as a random effect. A second ANOVA was performed with the addition of age, gender and the cube-root of WML volume as co-variables to determine if these factors could explain any variance in K^{trans} and v_p . Where significant group differences were found, post-hoc t-tests were performed with Bonferroni correction where stated. Statistical analyses were conducted using R 3.6.0 (R Core Team, 2019).

2.4.3 Correlation with cognitive and clinical parameters

Any association between the DCE-MRI parameters and cognitive deficit, medication and disease severity within the PD group was evaluated with a linear mixed effects model and ANOVA. Region (as a factor), MoCA score, LEDD dose and UPDRS score (as continuous variables) and their interaction with region were modelled as fixed effects, and subject was set as a random effect. Where significant interactions with region were found, the fixed effects t-tests and corresponding p values for each region were considered, calculated using Satterthwaite's approximation in the lmerTest package (54) in R 3.6.0 (R Core Team, 2019).

2.5 Data Availability

Data including images, imaging metrics and participant metadata are available on request. Please email the corresponding author: Laura.Parkes@manchester.ac.uk.

3. Results

Fifty-one PD patients were recruited, 17 CP subjects with cerebrovascular disease (13 with ischemic stroke, 4 with single or multiple transient ischaemic attacks; mean time since symptom onset and where applicable most recent known transient ischaemic attack = 1.1 ± 0.7 years) and 34 CN subjects. Twenty-eight participants were scanned at Salford Royal Hospital and 74 participants at the Manchester Clinical Research Facility (37 PD, 20 CN and 17 CP).

Data from 7 participants could not be analysed due to i) participants not tolerating the complete scan procedure (n=2) ii) failure of the contrast agent injection (n=3), resulting in either absent, very low or very distorted vascular input function and iii) non-physiological values of plasma volume (n=2); leaving data from 95 participants (49 PD, 31 CN, 15 CP). Summary demographic information from these patients is given in Table 1, along with the WML volume measurements. There were no significant differences in age between the groups. As expected the CP group had more cerebrovascular risk factors than either the PD or CN groups but there was no difference in risk factors between the PD and CN groups. WML volume was significantly higher in the PD group than the CN group, suggesting that, although vascular risk factors are similar, there was increased microvascular pathology in the PD group. WML volume was also higher in the CP group than the CN group, as expected, but not significantly different from the PD group. The PD group had significantly lower MoCA score compared to the CN group, but was not significantly different from the CP group. It is noted that there are significant gender differences between the PD and CN groups, which is addressed directly in a sub-analysis (see Supplementary Materials).

3.1 Voxel-wise analysis

Figure 2 shows mean images of K^{trans} and v_p in the three groups. It can be seen that K^{trans} is generally higher in PD than in the control groups. The v_p maps look similar between the PD and CN group, but the CP group has noticeably lower v_p .

The voxel-wise comparisons revealed significantly higher K^{trans} in the PD group than in the CN group (Figure 3 and Table S1) in regions including white matter regions of the precuneus bilaterally. Only the largest region in the right pre-cuneus survived cluster-level FWE correction. There were no regions of significantly lower K^{trans} in PD than in CN. K^{trans} was also significantly higher in the PD group than in the CP group in one region of white matter in the right temporal lobe (Table S2). Significantly higher K^{trans} was also seen in the CP group than in the CN group (Table S3), in the mid cingulum and R cerebellum. Aside from for the PD vs CN comparison, none of these regions survived the cluster-level FWE correction.

CP showed regions of significantly lower v_p than CN (Table S4) and PD (Table S5) in white matter regions of the left and right temporal lobes. No significant voxel-wise differences in v_p were seen for PD vs CN.

3.2 ROI Analysis

Figure 4 shows group mean regional values for K^{trans} and v_p . There was a significant effect of group ($F = 3.3$, $p = 0.04$) and region ($F = 54.1$, $p < 0.0001$) on K^{trans} with post-hoc tests showing K^{trans} to be significantly higher in PD than in CN ($p=0.03$, Bonferroni corrected) and no significant differences between the other two pairwise comparisons. The NAWM, posterior cortex and SN show elevated K^{trans} in PD compared to CN when considering differences on a region-by-region basis ($p<0.05$,

uncorrected). K^{trans} is also higher *within* the WML in PD in comparison to CN. A second ANOVA with WML volume, age and gender included as covariates showed a similar effect of group ($F = 3.9$, $p=0.02$) and region ($F = 54.1$, $p<0.0001$) and no significant effect of WML volume ($F=1.0$, $p=0.3$), age ($F=1.1$, $p=0.3$) or gender ($F=0.1$, $p=0.8$). Post-hoc tests again showed K^{trans} to be significantly higher in PD than in CN ($p=0.02$, Bonferroni corrected).

There was a significant effect of region ($F=90.0$, $p < 0.0001$) but not group ($F = 1.1$, $p = 0.3$) on v_p . The second ANOVA with WML volume, age and gender included as covariates showed a similar result with an impact of region ($F = 90.0$, $p<0.0001$) but not group ($F = 1.1$, $p=0.3$) on v_p and no significant effect of WML volume ($F=0.1$, $p=0.8$), age ($F=2.2$, $p=0.1$) or gender ($F=0.2$, $p=0.6$).

To check that differences were not driven by the differences in gender-matching or by the use of two scanners, the regional analysis was repeated with gender-matched groups and with data from only one scanner. Broadly the same regional and group effects were seen for both K^{trans} and v_p (see supplementary materials).

3.3 Correlation with cognitive and clinical parameters

Table 2 summaries the ANOVA findings evaluating the impact of cognitive deficit (MoCA score), medication (LEDD dose) and disease severity (UPDRS score) on the DCE-MRI parameters within the PD group. There are no significant associations between these parameters and K^{trans} . In particular, LEDD dose was not associated with K^{trans} suggesting that the increased BBB leakage seen in the PD group is not a consequence of medication. A significant effect of LEDD dose on v_p was found with higher LEDD dose associated with higher v_p .

4. Discussion

The aim of this study was to determine alterations in BBB permeability in PD, by comparison with controls, and to investigate whether potential changes are simply attributable to co-existing cerebrovascular disease in an aging population or if a pattern of BBB alteration specific to PD is revealed. The results show higher K^{trans} , reflecting higher BBB leakage, in PD than in CN (Figure 2 and 3 and Table S1), with a somewhat different spatial pattern to the differences seen between individuals with known cerebrovascular disease (CP) and CN (Table S3). Direct comparison of PD and CP shows higher K^{trans} for PD in the white matter of the right temporal lobe (Table S2). Blood plasma volume, v_p , is similar in PD and CN, with some evidence of lower v_p in the CP group (Table S4 and S5 and Figure 4). Collectively these data demonstrate BBB disruption in PD can be detected in the clinical setting in keeping with evidence from studies in animal models and post mortem human brain. The K^{trans} values (Figure 4) are within the wide range of published values which seem dependent on the specific acquisition and analysis methods and contrast agents used (55). A study using the same contrast agent and similar method shows very comparable values (56).

Both the voxel-based and the ROI analysis showed higher K^{trans} in PD when compared with CN. These results are in keeping with several studies showing altered components of the BBB in PD (27, 57-59) such as loss of capillaries, an alteration in the capillary caliber and thickened basement membrane (making the BBB less competent) (16). Our voxel-based analysis approach allows a whole brain view of BBB dysfunction, and, in the whole brain maps, we see a fairly diffuse pattern of BBB disruption in PD, compared to CN. K^{trans} differences only reach statistical significance in posterior regions; however, given the requirement for multiple comparisons correction, it would likely require

a much larger study for smaller brain regions such as basal ganglia nuclei to survive the statistical threshold. The ROI approach focused on areas expected to display disease pathology based on our understanding of the pathophysiology of PD. It revealed K^{trans} to be generally higher in the PD group than in the CN group. Considering the magnitude and significance of regional K^{trans} differences between PD and CN (Figure 4), this is driven mainly by differences in SN, NAWM, WML and the posterior cortex. Alterations in SN and posterior cortex are in keeping with BBB breakdown playing a role in the pathophysiology of PD.

The increased K^{trans} in posterior cortical regions in PD is particularly noteworthy as these are the same regions that display hypoperfusion (33, 34, 53, 60) i.e. the results strengthen the argument of a link between BBB leakage and hypoperfusion. Hypoperfusion has been attributed to altered vasculature (string vessels, shorter/loss of capillaries, tortuous vessels), which can hinder normal BBB function (25, 28, 30, 61). BBB disruption has been attributed to alterations in key components such as tight junctions, potentially caused by pro-inflammatory cytokines and altered vascular endothelial growth factor (VEGF) (62-64). Interestingly a study using albumin (mg/L)/plasma albumin (g/L) ratio in the cerebral spinal fluid (CSF) to measure BBB dysfunction, revealed increased BBB dysfunction in PD compared to controls which was associated with increased CSF biomarkers of angiogenesis (e.g. VEGF) (22). These substances can also alter perfusion, with enhanced angiogenesis resulting in abnormal vascular permeability in PD. Future longitudinal imaging studies will be important to understand whether hypoperfusion leads to altered BBB function, or vice versa, or in fact whether BBB and perfusion changes have a common cause, for example, inflammation. Furthermore, it will be important to determine what downstream effects these microvascular changes may have on neuronal loss. We did not observe any statistically significant differences in K^{trans} between CP and CN unlike other studies which have reported elevated K^{trans} post-stroke (43). However, the small sample size and high heterogeneity of the CP group may have contributed to this.

WML have been used as a surrogate marker of SVD (65). We find higher WML volume in the PD group than the CN group despite the fact the groups have no significant differences in cardiovascular risk factors. Previous studies of WML in PD however show mixed results (66, 67). To investigate whether the WML volume was driving the K^{trans} group differences, we used ANOVA with WML volume, age, and gender as co-variables and found that there was no significant association between WML volume (or age or gender) and K^{trans} . The main finding of higher K^{trans} in the PD group than CN was maintained. Recent work has tried to understand the link between BBB dysfunction and WML revealing a continuum of BBB disruption leading to myelin loss and fibrinogen accumulation resulting in WML formation (68-70). Indeed NAWM (particularly that surrounding the WML) has been shown to have increased BBB leakage suggesting BBB disruption can precede WML formation (43). We do not find a significant association between WML volume and K^{trans} , which alongside the higher K^{trans} in NAWM in the PD group compared to CN, supports this notion that BBB disruption is diffuse throughout the white matter and perhaps precedes WML formation. It is interesting to note that, within the lesions, K^{trans} is significantly higher in the PD group than in the CN group suggesting more severe underlying pathology.

Our measurements of blood plasma volume, v_p are not significantly different between PD and healthy controls, which may seem contradictory to the well-reported hypoperfusion in PD, given that blood volume and perfusion are closely related. However, blood flow also depends on the blood velocity within the capillaries which may underlie the observed differences. Indeed, we have previously found significantly prolonged arterial transit time in posterior brain regions in PD,

suggesting lower blood velocity (53). Furthermore, v_p estimation may also be affected by the rate of trans-endothelial water exchange leading to possible underestimation of v_p in the CN group in comparison to the PD group due to the relatively more intact BBB, potentially contributing to the lack of group difference seen. As the K^{trans} and v_p patterns differed between CP and PD this would suggest that the BBB alterations do not simply occur due to co-existing cerebrovascular disease (indeed PD patients with known cerebrovascular disease were not included in the study and the PD group had significantly fewer cerebrovascular risk factors) but plays an independent role in PD pathophysiology. Together with the increased WML volume in the PD group, this supports the hypothesis that microvascular pathology occurs in PD.

We explored the impact of cognitive deficit (MoCA score), medication (LEDD dose) and disease severity (UPDRS score) on K^{trans} and v_p within the PD group. LEDD dose was associated with higher v_p , which is in keeping with studies that suggest L-dopa increases blood flow in certain regions (71, 72). There were no significant associations between any parameter and K^{trans} and we conclude that the K^{trans} differences between the PD and CN groups are not driven by the differences in MoCA score or by levodopa medications.

One limitation of this study is the significant gender imbalance between the PD and CN groups (Table 1) with relatively more men in the PD group. However, we do not believe this compromises our findings as there are no reports of gender differences in K^{trans} values, and secondary analysis of our own data shows consistent findings in a gender-matched sub-group (Supplementary Materials). Likewise we collected data on two different scanners which may have influenced the results; however secondary analysis shows consistent findings in findings from a single scanner (Supplementary Materials). We interpret the higher K^{trans} in PD as relating to higher endothelial leakage, but note that K^{trans} is also affected by cerebral blood flow. However cerebral blood flow is lower than normal in posterior regions in PD (27, 29, 30, 46) which would lead to lower K^{trans} , and yet we see higher K^{trans} in the PD group, implying that the differences are not due to blood flow differences.

In conclusion, this study has shown subtle BBB disruption in PD, in key regions implicated in the pathophysiology including the substantia nigra, white matter and posterior cortical regions. Further research is needed, including longitudinal clinical imaging studies combining neuronal, metabolic and vascular measurements to better understand disease mechanisms and so identify potential therapeutic targets in PD.

The authors declare that the research was conducted in the absence of any commercial or financial relationships that could be construed as a potential conflict of interest.

Author Contributions

(1) Study: A = conception; B = organization; C = execution; (2) Data: A = collection; B = analysis; C = interpretation; (3) Manuscript: A = writing the first draft; B = reviewing the manuscript.

S.A.: 1A, 1B, 1C, 2A, 2B, 2C, 3A, 3B

J.N.: 2B, 2C, 3B

G.P.: 1C, 2C, 3B

H.E.: 1A, 1B, 1C, 2C, 3A, 3B

397 L.P: 1A, 1B, 1C, 2B, 2C, 3A, 3B

398 **Funding**

399 Salary (Dr Al-Bachari) and research costs for this work were provided through support from:
 400 University of Lancaster, Sydney Driscoll Neuroscience Foundation, University of Manchester and
 401 Medical Research Council Studentship, Lancashire Teaching Hospitals NHS Foundation Trust, and
 402 the Engineering and Physical Science Research Council (EP/M005909/1). Professor Emsley is
 403 supported by Lancashire Teaching Hospitals NHS Foundation Trust and Lancaster University. Drs
 404 Parkes and Naish and Professor Parker were supported by the University of Manchester.
 405

406 **References:**

- 407 1. Pardridge WM. Molecular biology of the blood-brain barrier. *Mol Biotechnol.* 2005;30(1):57-
 408 70.
- 409 2. Alvarez JI, Katayama T, Prat A. Glial influence on the blood brain barrier. *Glia.*
 410 2013;61(12):1939-58.
- 411 3. Lo EH, Rosenberg GA. The neurovascular unit in health and disease: introduction. *Stroke.*
 412 2009;40(3 Suppl):S2-3.
- 413 4. Zlokovic BV. Neurovascular pathways to neurodegeneration in Alzheimer's disease and other
 414 disorders. *Nat Rev Neurosci.* 2011;12(12):723-38.
- 415 5. Zlokovic BV. The blood-brain barrier in health and chronic neurodegenerative disorders.
 416 *Neuron.* 2008;57(2):178-201.
- 417 6. Bell RD, Winkler EA, Sagare AP, Singh I, LaRue B, Deane R, et al. Pericytes control key
 418 neurovascular functions and neuronal phenotype in the adult brain and during brain aging. *Neuron.*
 419 2010;68(3):409-27.
- 420 7. Montagne A, Nikolakopoulou AM, Zhao Z, Sagare AP, Si G, Lazic D, et al. Pericyte
 421 degeneration causes white matter dysfunction in the mouse central nervous system. *Nature medicine.*
 422 2018;24(3):326-37.
- 423 8. Collins LM, Toulouse A, Connor TJ, Nolan YM. Contributions of central and systemic
 424 inflammation to the pathophysiology of Parkinson's disease. *Neuropharmacology.* 2012;62(7):2154-
 425 68.
- 426 9. Carvey PM, Punati A, Newman MB. Progressive dopamine neuron loss in Parkinson's
 427 disease: the multiple hit hypothesis. *Cell Transplant.* 2006;15(3):239-50.
- 428 10. Sweeney MD, Zhao Z, Montagne A, Nelson AR, Zlokovic BV. Blood-Brain Barrier: From
 429 Physiology to Disease and Back. *Physiological reviews.* 2019;99(1):21-78.
- 430 11. Andreone BJ, Lacoste B, Gu C. Neuronal and vascular interactions. *Annu Rev Neurosci.*
 431 2015;38:25-46.
- 432 12. Grammas P, Martinez J, Miller B. Cerebral microvascular endothelium and the pathogenesis
 433 of neurodegenerative diseases. *Expert Rev Mol Med.* 2011;13:e19.
- 434 13. Zhao Z, Nelson AR, Betsholtz C, Zlokovic BV. Establishment and Dysfunction of the Blood-
 435 Brain Barrier. *Cell.* 2015;163(5):1064-78.

- 436 14. Nelson AR, Sweeney MD, Sagare AP, Zlokovic BV. Neurovascular dysfunction and
437 neurodegeneration in dementia and Alzheimer's disease. *Biochim Biophys Acta*. 2015.
- 438 15. Hachinski V, Einhäupl K, Ganten D, Alladi S, Brayne C, Stephan BCM, et al. Special topic
439 section: linkages among cerebrovascular, cardiovascular, and cognitive disorders: Preventing
440 dementia by preventing stroke: The Berlin Manifesto. *Int J Stroke*. 2019;1747493019871915.
- 441 16. Brown WR, Thore CR. Review: cerebral microvascular pathology in ageing and
442 neurodegeneration. *Neuropathol Appl Neurobiol*. 2011;37(1):56-74.
- 443 17. Di Marco LY, Venneri A, Farkas E, Evans PC, Marzo A, Frangi AF. Vascular dysfunction in
444 the pathogenesis of Alzheimer's disease--A review of endothelium-mediated mechanisms and
445 ensuing vicious circles. *Neurobiol Dis*. 2015;82:593-606.
- 446 18. Iadecola C. The Neurovascular Unit Coming of Age: A Journey through Neurovascular
447 Coupling in Health and Disease. *Neuron*. 2017;96(1):17-42.
- 448 19. Kisler K, Nelson AR, Montagne A, Zlokovic BV. Cerebral blood flow regulation and
449 neurovascular dysfunction in Alzheimer disease. *Nat Rev Neurosci*. 2017;18(7):419-34.
- 450 20. Wada K, Arai H, Takanashi M, Fukae J, Oizumi H, Yasuda T, et al. Expression levels of
451 vascular endothelial growth factor and its receptors in Parkinson's disease. *Neuroreport*.
452 2006;17(7):705-9.
- 453 21. Faucheux BA, Bonnet AM, Agid Y, Hirsch EC. Blood vessels change in the mesencephalon
454 of patients with Parkinson's disease. *Lancet*. 1999;353(9157):981-2.
- 455 22. Janelidze S, Lindqvist D, Francardo V, Hall S, Zetterberg H, Blennow K, et al. Increased CSF
456 biomarkers of angiogenesis in Parkinson disease. *Neurology*. 2015;85(21):1834-42.
- 457 23. Patel A, Toia GV, Colletta K, Bradaric BD, Carvey PM, Hendey B. An angiogenic inhibitor,
458 cyclic RGDfV, attenuates MPTP-induced dopamine neuron toxicity. *Exp Neurol*. 2011;231(1):160-
459 70.
- 460 24. Farkas E, De Jong GI, de Vos RA, Jansen Steur EN, Luiten PG. Pathological features of
461 cerebral cortical capillaries are doubled in Alzheimer's disease and Parkinson's disease. *Acta*
462 *Neuropathol*. 2000;100(4):395-402.
- 463 25. Guan J, Pavlovic D, Dalkie N, Waldvogel HJ, O'Carroll SJ, Green CR, et al. Vascular
464 degeneration in Parkinson's disease. *Brain Pathol*. 2013;23(2):154-64.
- 465 26. Chao YX, He BP, Tay SS. Mesenchymal stem cell transplantation attenuates blood brain
466 barrier damage and neuroinflammation and protects dopaminergic neurons against MPTP toxicity in
467 the substantia nigra in a model of Parkinson's disease. *J Neuroimmunol*. 2009;216(1-2):39-50.
- 468 27. Barcia C, Bautista V, Sanchez-Bahillo A, Fernandez-Villalba E, Faucheux B, Poza y Poza M,
469 et al. Changes in vascularization in substantia nigra pars compacta of monkeys rendered
470 parkinsonian. *J Neural Transm (Vienna)*. 2005;112(9):1237-48.
- 471 28. Rite I, Machado A, Cano J, Venero JL. Blood-brain barrier disruption induces in vivo
472 degeneration of nigral dopaminergic neurons. *Journal of neurochemistry*. 2007;101(6):1567-82.
- 473 29. Kortekaas R, Leenders KL, van Oostrom JC, Vaalburg W, Bart J, Willemsen AT, et al.
474 Blood-brain barrier dysfunction in parkinsonian midbrain in vivo. *Ann Neurol*. 2005;57(2):176-9.
- 475 30. Gray MT, Woulfe JM. Striatal blood-brain barrier permeability in Parkinson's disease. *J*
476 *Cereb Blood Flow Metab*. 2015;35(5):747-50.

31. Borghammer P. Perfusion and metabolism imaging studies in Parkinson's disease. *Dan Med J*. 2012;59(6):B4466.
32. Ma Y, Huang C, Dyke JP, Pan H, Alsop D, Feigin A, et al. Parkinson's disease spatial covariance pattern: noninvasive quantification with perfusion MRI. *Journal of cerebral blood flow and metabolism : official journal of the International Society of Cerebral Blood Flow and Metabolism*. 2010;30(3):505-9.
33. Melzer TR, Watts R, MacAskill MR, Pearson JF, Rueger S, Pitcher TL, et al. Arterial spin labelling reveals an abnormal cerebral perfusion pattern in Parkinson's disease. *Brain*. 2011;134(Pt 3):845-55.
34. Fernandez-Seara MA, Mengual E, Vidorreta M, Aznarez-Sanado M, Loayza FR, Villagra F, et al. Cortical hypoperfusion in Parkinson's disease assessed using arterial spin labeled perfusion MRI. *NeuroImage*. 2012;59(3):2743-50.
35. Kamagata K, Motoi Y, Hori M, Suzuki M, Nakanishi A, Shimoji K, et al. Posterior hypoperfusion in Parkinson's disease with and without dementia measured with arterial spin labeling MRI. *J Magn Reson Imaging*. 2011;33(4):803-7.
36. Tofts PS, Kermode AG. Measurement of the blood-brain barrier permeability and leakage space using dynamic MR imaging. 1. Fundamental concepts. *Magn Reson Med*. 1991;17(2):357-67.
37. Wardlaw JM, Farrall A, Armitage PA, Carpenter T, Chappell F, Doubal F, et al. Changes in background blood-brain barrier integrity between lacunar and cortical ischemic stroke subtypes. *Stroke*. 2008;39(4):1327-32.
38. Starr JM, Farrall AJ, Armitage P, McGurn B, Wardlaw J. Blood-brain barrier permeability in Alzheimer's disease: a case-control MRI study. *Psychiatry Res*. 2009;171(3):232-41.
39. Montagne A, Barnes SR, Sweeney MD, Halliday MR, Sagare AP, Zhao Z, et al. Blood-brain barrier breakdown in the aging human hippocampus. *Neuron*. 2015;85(2):296-302.
40. Taheri S, Gasparovic C, Huisa BN, Adair JC, Edmonds E, Prestopnik J, et al. Blood-brain barrier permeability abnormalities in vascular cognitive impairment. *Stroke*. 2011;42(8):2158-63.
41. Starr JM, Wardlaw J, Ferguson K, MacLulich A, Deary IJ, Marshall I. Increased blood-brain barrier permeability in type II diabetes demonstrated by gadolinium magnetic resonance imaging. *J Neurol Neurosurg Psychiatry*. 2003;74(1):70-6.
42. Heye AK, Culling RD, Valdés Hernández MdC, Thrippleton MJ, Wardlaw JM. Assessment of blood-brain barrier disruption using dynamic contrast-enhanced MRI. A systematic review. *NeuroImage: Clinical*. 2014;6:262-74.
43. Wardlaw JM, Makin SJ, Valdés Hernández MC, Armitage PA, Heye AK, Chappell FM, et al. Blood-brain barrier failure as a core mechanism in cerebral small vessel disease and dementia: evidence from a cohort study. *Alzheimers Dement*. 2017;13(6):634-43.
44. Emre M, Aarsland D, Brown R, Burn DJ, Duyckaerts C, Mizuno Y, et al. Clinical diagnostic criteria for dementia associated with Parkinson's disease. *Mov Disord*. 2007;22(12):1689-707; quiz 837.
45. Hoehn MM, Yahr MD. Parkinsonism: onset, progression and mortality. *Neurology*. 1967;17(5):427-42.
46. Tomlinson CL, Stowe R, Patel S, Rick C, Gray R, Clarke CE. Systematic review of levodopa dose equivalency reporting in Parkinson's disease. *Mov Disord*. 2010;25(15):2649-53.

47. Wardlaw JM, Smith EE, Biessels GJ, Cordonnier C, Fazekas F, Frayne R, et al. Neuroimaging standards for research into small vessel disease and its contribution to ageing and neurodegeneration. *Lancet Neurology*. 2013;12(8):822-38.
48. Schmidt P, Gaser C, Arsic M, Buck D, Förschler A, Berthele A, et al. An automated tool for detection of FLAIR-hyperintense white-matter lesions in Multiple Sclerosis. *Neuroimage*. 2012;59(4):3774-83.
49. Stefaniak JD, Parkes LM, Parry- Jones AR, Potter GM, Vail A, Jovanovic A, et al. Enzyme replacement therapy and white matter hyperintensity progression in Fabry disease. *Neurology*. 2018; 91(15):e1413–e22.
50. Lavini C, Verhoeff JJ. Reproducibility of the gadolinium concentration measurements and of the fitting parameters of the vascular input function in the superior sagittal sinus in a patient population. *Magn Reson Imaging*. 2010;28(10):1420-30.
51. Tzourio-Mazoyer N, Landeau B, Papathanassiou D, Crivello F, Etard O, Delcroix N, et al. Automated anatomical labeling of activations in SPM using a macroscopic anatomical parcellation of the MNI MRI single-subject brain. *NeuroImage*. 2002;15(1):273-89.
52. Prodoehl J, Yu H, Little DM, Abraham I, Vaillancourt DE. Region of interest template for the human basal ganglia: comparing EPI and standardized space approaches. *NeuroImage*. 2008;39(3):956-65.
53. Al-Bachari S, Vidyasagar R, Emsley HC, Parkes LM. Structural and physiological neurovascular changes in idiopathic Parkinson's disease and its clinical phenotypes. *J Cereb Blood Flow Metab*. 2017;37(10):3409-21.
54. Kuznetsova A, Brockhoff PB, Christensen RHB. lmerTest Package: Tests in Linear Mixed Effects Models. 2017. 2017;82(13):26.
55. Raja R, Rosenberg GA, Caprihan A. MRI measurements of Blood-Brain Barrier function in dementia: A review of recent studies. *Neuropharmacology*. 2018;134(Pt B):259-71.
56. Heye AK, Thrippleton MJ, Armitage PA, Valdés Hernández MDC, Makin SD, Glatz A, et al. Tracer kinetic modelling for DCE-MRI quantification of subtle blood-brain barrier permeability. *Neuroimage*. 2016;125:446-55.
57. Carvey PM, Zhao CH, Hendey B, Lum H, Trachtenberg J, Desai BS, et al. 6-Hydroxydopamine-induced alterations in blood-brain barrier permeability. *Eur J Neurosci*. 2005;22(5):1158-68.
58. Chao YX, He BP, Tay SSW. Mesenchymal stem cell transplantation attenuates blood brain barrier damage and neuroinflammation and protects dopaminergic neurons against MPTP toxicity in the substantia nigra in a model of Parkinson's disease. *Journal of neuroimmunology*. 2009;216(1-2):39-50.
59. Sarkar S, Raymick J, Mann D, Bowyer JF, Hanig JP, Schmued LC, et al. Neurovascular changes in acute, sub-acute and chronic mouse models of Parkinson's disease. *Curr Neurovasc Res*. 2014;11(1):48-61.
60. Borghammer P, Chakravarty M, Jonsdottir KY, Sato N, Matsuda H, Ito K, et al. Cortical hypometabolism and hypoperfusion in Parkinson's disease is extensive: probably even at early disease stages. *Brain Struct Funct*. 2010;214(4):303-17.
61. Fang X. Impaired tissue barriers as potential therapeutic targets for Parkinson's disease and amyotrophic lateral sclerosis. *Metabolic brain disease*. 2018;33(4):1031-43.

62. Matsumoto J, Stewart T, Sheng L, Li N, Bullock K, Song N, et al. Transmission of alpha-synuclein-containing erythrocyte-derived extracellular vesicles across the blood-brain barrier via adsorptive mediated transcytosis: another mechanism for initiation and progression of Parkinson's disease? *Acta Neuropathol Commun.* 2017;5(1):71.
63. Chen C, Li X, Ge G, Liu J, Biju KC, Laing SD, et al. GDNF-expressing macrophages mitigate loss of dopamine neurons and improve Parkinsonian symptoms in MitoPark mice. *Scientific reports.* 2018;8(1):5460.
64. Carvey PM, Hendey B, Monahan AJ. The blood-brain barrier in neurodegenerative disease: a rhetorical perspective. *J Neurochem.* 2009;111(2):291-314.
65. Wardlaw JM, Smith EE, Biessels GJ, Cordonnier C, Fazekas F, Frayne R, et al. Neuroimaging standards for research into small vessel disease and its contribution to ageing and neurodegeneration. *Lancet Neurol.* 2013;12(8):822-38.
66. de Schipper LJ, Hafkemeijer A, Bouts M, van der Grond J, Marinus J, Henselmans JML, et al. Age- and disease-related cerebral white matter changes in patients with Parkinson's disease. *Neurobiol Aging.* 2019;80:203-9.
67. Rabbitt PM, Scott M, Thacker N, Lowe C, Horan M, Pendleton N, et al. Balance marks cognitive changes in old age because it reflects global brain atrophy and cerebro-arterial blood-flow. *Neuropsychologia.* 2006;44(10):1978-83.
68. Wardlaw JM. William M. Feinberg Award for Excellence in Clinical Stroke: Small Vessel Disease; a Big Problem, But Fixable. *Stroke.* 2018;49(7):1770-5.
69. Muñoz Maniega S, Chappell FM, Valdés Hernández MC, Armitage PA, Makin SD, Heye AK, et al. Integrity of normal-appearing white matter: Influence of age, visible lesion burden and hypertension in patients with small-vessel disease. *J Cereb Blood Flow Metab.* 2017;37(2):644-56.
70. Wardlaw JM, Smith C, Dichgans M. Small vessel disease: mechanisms and clinical implications. *Lancet Neurol.* 2019;18(7):684-96.
71. Ohlin KE, Sebastianutto I, Adkins CE, Lundblad C, Lockman PR, Cenci MA. Impact of L-DOPA treatment on regional cerebral blood flow and metabolism in the basal ganglia in a rat model of Parkinson's disease. *NeuroImage.* 2012;61(1):228-39.
72. Ko JH, Lerner RP, Eidelberg D. Effects of levodopa on regional cerebral metabolism and blood flow. *Mov Disord.* 2015;30(1):54-63.

Tables

Table 1: Demographics and clinical and radiological characteristics of the study group

	CN (n=31)	CP (n=15)	PD (n=49)	p value PD v CN	p value PD v CP	p value CP v CN
n (F:M)	16:15	4:11	12:37	0.01	0.25	0.07
Age (years): mean (range)	66.4 (52-81)	69.1 (53-84)	68.9 (52-85)	0.23	0.84	0.26
No. of cardiovascular risk factors: mean (SD)	1.52 (1.12)	2.93 (1.16)	1.72 (1.52)	0.55	0.002	<0.0001
Cardiovascular Risk Factors (% of group):						
Hypertension	29.0	73.3	26.5	0.13	0.02	0.005
Diabetes mellitus	6.5	13.3	6.1	0.36	0.43	0.46
FH of CVD	45.2	46.7	22.4	0.10	0.15	0.25
Smoker	29.0	66.7	28.6	0.15	0.03	0.01
Hypercholesterolaemia	45.2	68.9	22.4	0.08	0.004	0.05
Ischaemic heart disease	6.5	13.3	12.2	0.13	0.31	0.30
Atrial fibrillation	0	20.0	2.0	0.61	0.04	0.03
Disease Duration (years): mean (SD)	N/A	1.1 (0.77)	7.2 (4.45)	N/A	N/A	N/A
Hoehn & Yahr Score: mean (SD)	N/A	N/A	2.60 (0.09)	N/A	N/A	N/A
UPDRS Score: mean (SD)	N/A	N/A	29.2 (12.7)	N/A	N/A	N/A
LEDD (mg): mean (SD)	N/A	N/A	583.5 (399.6)	N/A	N/A	N/A
MoCA Score: mean (SD)	27.9 (2.3)	26.1 (2.9)	25.2 (3.9)	0.0004	0.39	0.04
Cube-root of WML volume (mm): mean (SD)	1.26 (0.83)	2.11 (0.72)	1.80 (0.95)	0.008	0.19	0.001

AF: atrial fibrillation; CN: control negative; CP: control positive; CV: cardiovascular; DM: diabetes mellitus; FH of CVD: family history of cardiovascular disease; Hyperchol.: hypercholextrolaemia; IHD: ischaemic heart disease; LEDD: levodopa equivalent daily dose; MoCA: Montreal Cognitive Assessment; RF: risk factors; PD: Parkinson's disease; TD: tremor dominant; UPDRS 111: unified Parkinson's disease rating scale motor score; WML: white matter lesion.

Table 2: Analysis of variance for the impact of cognitive deficit (MoCA score), medication (LEDD dose) and disease severity (UPDRS score) on regional DCE-MRI parameters within the PD group.

Factor		K^{trans} as dependent variable		V_p as dependent variable	
	Deg. freedom	F value	P value	F value	P value
Region	6	0.3	1.0	3.5	0.002
MoCA	1	3.8	0.06	0.4	0.52
LEDD	1	0.4	0.5	6.1	0.02
UPDRS	1	0.5	0.5	0.02	0.9
Region:MoCA	6	0.1	1.0	1.7	0.1
Region:LEDD	6	0.5	0.8	1.0	0.4
Region: UPDRS	6	0.4	0.9	0.8	0.5

Figure Captions

Figure 1: Location of the regions of interest

Figure 2: Mean images of K^{trans} and v_p for each group

Images of the mean contrast agent transfer coefficient K^{trans} and the plasma volume v_p for each group. Individual images were first normalised to MNI space before averaging. A T₁-weighted image is shown for reference.

Figure 3: Regions of higher K^{trans} in the PD group compared to the CN group

t-statistic map overlaid on structural image showing the regions of significantly higher K^{trans} in the PD group than in the CN group. Map is thresholded with voxel-level $p < 0.001$ (uncorrected) and minimum cluster size of 50 voxels. The arrow indicates the cluster that survives cluster-level family-wise error correction for multiple comparisons ($p < 0.05$).

Figure 4: Mean values for K^{trans} and v_p in regions of interest for each group

Mean values are given for the (A) the contrast agent transfer coefficient K^{trans} and (B) the plasma volume v_p . Error bars show the standard error in the mean. The significance of post-hoc t-tests (uncorrected) between K^{trans} in the PD and CN group are shown. SN = substantia nigra, CA= caudate, PU = putamen, P = pallidum, WML = white matter lesions, NAWM = normal-appearing white matter, FC = frontal cortex, PC = posterior cortices

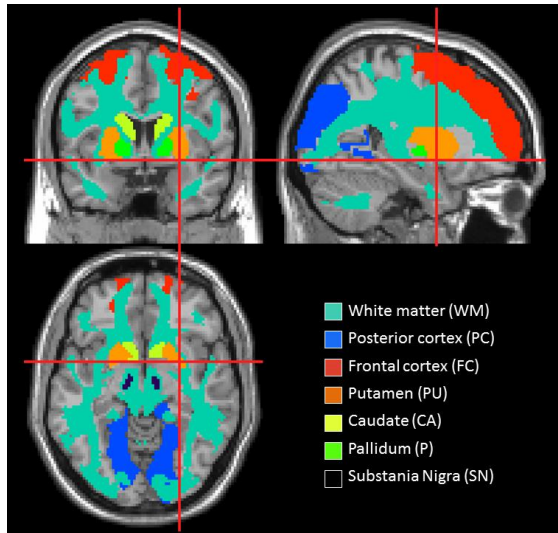


Figure 1: Location of the regions of interest

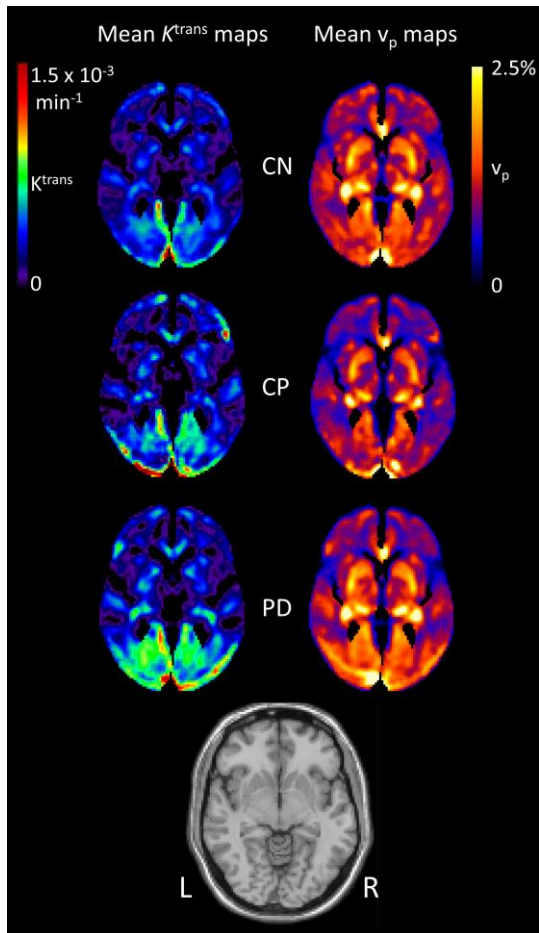


Figure 2: Mean images of K^{trans} and v_p for each group

Images of the mean contrast agent transfer coefficient K^{trans} and the plasma volume v_p for each group. Individual images were first normalised to MNI space before averaging. A T₁-weighted image is shown for reference.

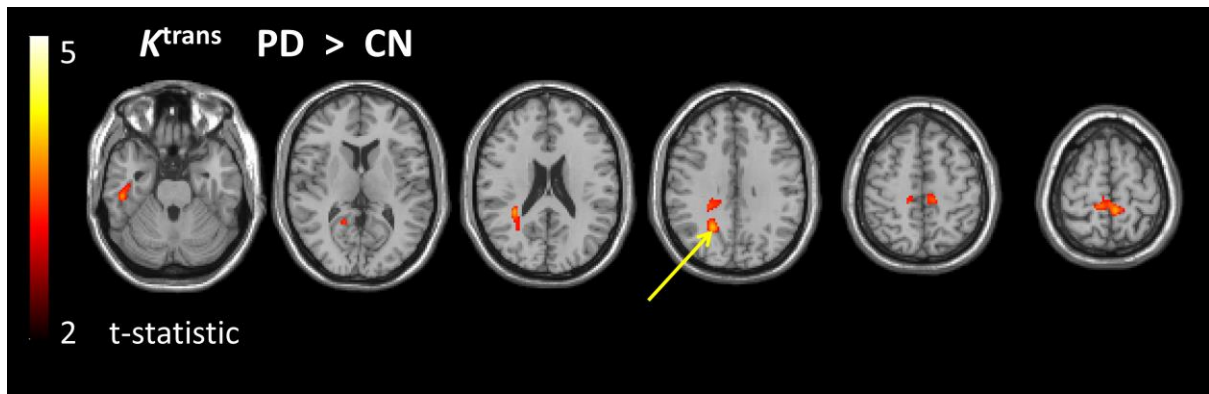


Figure 3: Regions of higher K^{trans} in the PD group compared to the CN group

t-statistic map overlaid on structural image showing the regions of significantly higher K^{trans} in the PD group than in the CN group. Map is thresholded with voxel-level $p < 0.001$ (uncorrected) and minimum cluster size of 50 voxels. The arrow indicates the cluster that survives cluster-level family-wise error correction for multiple comparisons ($p < 0.05$).

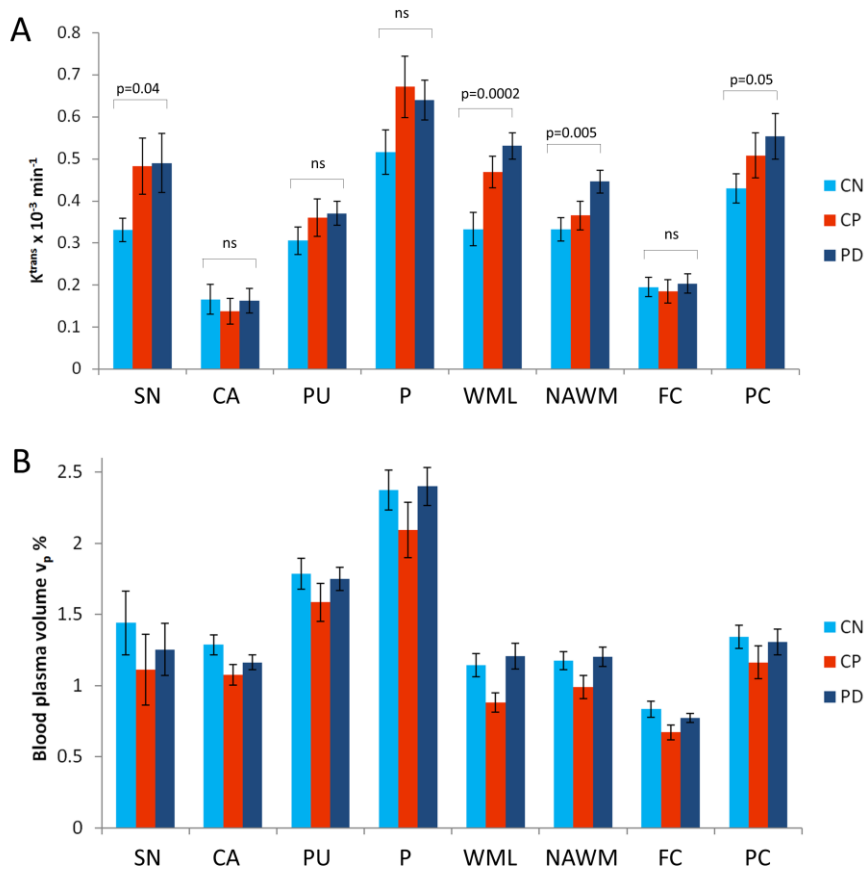


Figure 4: Mean values for K^{trans} and v_p in regions of interest for each group

Mean values are given for the (A) the contrast agent transfer coefficient K^{trans} and (B) the plasma volume v_p . Error bars show the standard error in the mean. The significance of post-hoc t-tests (uncorrected) between K^{trans} in the PD and CN group are shown. SN = substantia nigra, CA= caudate, PU = putamen, P = pallidum, WML = white matter lesions, NAWM = normal-appearing white matter, FC = frontal cortex, PC = posterior cortices

Supplementary Material

1. Methods

Further detail of MRI acquisition protocol and analysis is outlined below.

1.1 MRI acquisition protocol

A DCE-MRI dynamic series of 3D T_1 -fast field echo (T_1 -FFE) were acquired with the following scan parameters: Field of view 192 mm x 192 mm and matrix size of 128 giving in-plane resolution of 1.5 x 1.5 mm; 32 contiguous axial slices of 4 mm thickness; echo time (TE) = 0.8 ms, repetition time (TR) = 2.4 ms, flip angle 10 degrees and image acquisition time of 7.6 seconds. 160 images were acquired over approximately 20 minutes.

Prior to the dynamic scan, a series of additional 3D T_1 -FFE images were acquired at 3 flip angles (2, 5 and 10 degrees) in order to calculate a pre-contrast T_1 map using the variable flip angle method (1), with geometry and all other parameters matched to the dynamic series, except only 8 image repeats were collected (from which a mean image was created), giving an acquisition time of 60 s per flip angle. In order to correct for B_1 field inhomogeneities, a B_1 mapping sequence (2) was also acquired with the same voxel size and coverage as for the variable flip angle images. This consisted of a pair of 3D spoiled gradient echo images with $TR_1 = 25$ ms and $TR_2 = 125$ ms, flip angle 60 degrees, TE = 5 ms, acquisition time 117 seconds.

In addition, a T_2 -weighted FLAIR image was acquired with the following parameters: TR = 10 s, inversion time 2.75 s, TE = 140 ms, in-plane resolution of 0.69 mm x 0.69 mm, and 100 contiguous axial slices of 1.3 mm thickness with an acquisition time of 450 seconds. A 3D T_1 -weighted image was also collected with scan parameters: TR = 8.4 ms, TE = 3.9 ms, flip angle 8 degrees. Images were reconstructed with a resolution of 0.94 mm x 0.94 mm x 1mm, acquisition time 311 seconds.

1.2 MRI analysis

A voxel-by-voxel fit of the dynamic data for both the contrast agent transfer coefficient (K^{trans}) and plasma volume (v_p) was performed using the 'Patlak' model:

$$C_t(t) = K^{trans} \int_0^t C_p(t') dt' + v_p C_p(t) \quad [1]$$

Where $C_t(t)$ is the tissue concentration of the contrast agent and $C_p(t)$ is the plasma concentration at time t after contrast agent injection at $t=0$.

The tissue concentration $C_t(t)$ is calculated from the signal in the dynamic images $S_t(t)$ according to:

$$C_{t,b}(t) = \frac{R_1(t) - R_{10}}{r_1} \quad [2]$$

Where $R_1(t)$ is calculated from $S_t(t)$ as described subsequently in equation 5. Where r_1 is the longitudinal relaxivity of the contrast agent, which was assumed to be $3.4 \text{ s}^{-1} \text{ mM}^{-1}$. R_{10} is the baseline longitudinal relaxation rate, taken from the pre-contrast T_1 map using $R_{10} = 1/T_{10}$.

This pre-contrast T_1 map was calculated by fitting the variable flip angle images on a voxel-by-voxel basis for T_{10} and A_0 using equation [3] (1):

$$S = \frac{A_0 \sin \theta (1 - e^{-TR/T_{10}})}{1 - \cos \theta e^{-TR/T_{10}}} \quad [3]$$

In order to correct for inaccuracies in the specified flip angles, θ_s , due to B_1 inhomogeneities, the ratio of the image intensities in the B_1 mapping sequence (r) was used to estimate the true flip angle θ_T on a voxel-by-voxel basis (3), using:

$$\theta_T = \cos^{-1} \left(\frac{r \cdot n - 1}{n - r} \right) \quad \text{where } n = TR_1/TR_2. \quad [4]$$

The deviation of the true flip angle from the specified flip angle (θ_s) is given by θ_T/θ_s and θ in equation [3] is multiplied by this factor on a voxel wise basis when calculating T_1 . Prior to multiplication, the θ_T/θ_s image was smoothed using a convolution kernel of 3 voxels.

$R_1(t)$ was calculated using equation [5] below, derived from equation [3], considering S_t as the signal in the post-contrast dynamic images and S_0 as the mean signal from 5 pre-contrast dynamics, ignoring the first image due to equilibrium effects.

$$R_1(t) = -\frac{1}{TR} \ln \left[\frac{1 - B \cos \theta + \frac{S_t(t)}{S_0} (B - 1)}{1 - B \cos \theta + \frac{S_t(t)}{S_0} \cos \theta (B - 1)} \right] \quad \text{where } B = \exp(-R_{10} \cdot TR). \quad [5]$$

Finally, the plasma concentration $C_p(t)$, is derived from the blood concentration $C_b(t)$ which is also calculated using equations [2] and [5] with S_t the mean signal from the sagittal sinus region, S_0 the mean signal from 5 pre-contrast dynamics within this region (again, neglecting the first one to avoid inflow effects), and T_{10} equal to the mean pre-contrast T_1 from the sagittal sinus region. $C_p(t)$ is derived from the measured blood concentration by correcting for hematocrit according to: $C_p(t) = C_b(t) / (1 - \text{Hct})$ where Hct of 0.40 was used for a female and 0.45 for male (4).

Equation [1] was then fit to $C_t(t)$ and $C_p(t)$ using constrained least squares minimisation (lsqcurvefit in Matlab) on a voxel-wise basis for 3 parameters: K^{trans} , v_p and T_0 , where T_0 is the offset time between $C_t(t)$ and $C_p(t)$. K^{trans} was constrained to be between -0.001 min^{-1} and 0.1 min^{-1} , v_p between 0 and $(1 - \text{Hct})$ and T_0 between -20 and 20 s. The non-zero lower bound on K^{trans} , while un-physiological, is to avoid positive bias in the K^{trans} values which may in reality be very close to zero in healthy tissue. The negative bounds on T_0 are to allow for the possibility that the peak sagittal sinus signal may occur earlier than that of the regional blood circulation if blood takes a particularly tortuous path to the region. In order to avoid local minima, minimisation was performed twice, using the fitted parameters of the first minimisation as starting parameters for the second minimisation, except for one parameter which was kept as the original value.

Voxel-wise analysis was performed using the SPM12 PET toolbox to determine regional differences in K^{trans} and v_p between the groups. First we co-registered the K^{trans} and v_p maps to the high resolution 3D T_1 -weighted image: the first volume of the motion-corrected DCE series was used to compute the registration parameters which were then applied to the other images. Each T_1 -weighted image was segmented into tissue classes using SPM and grey and white matter masks were defined using a probability threshold of 75%. The co-registered

parameter maps were masked to include signal only from grey and white matter. The T_1 -weighted images were then normalized to Montreal Neurological Institute (MNI) space and the transformation applied to the K^{trans} and v_p maps.

1.3 Visual inspection of data quality

The DCE concentration time course in the white matter and the sagittal sinus regions (i.e. the VIF) were extracted for each person in order to consider individual differences in this raw data prior to fitting. For example, attention was paid to the shape and amplitude of the VIF in order to ascertain that the contrast agent injection was as expected.

Figure S1 shows example tissue concentration time courses for a representative person from each group, selected according to their K^{trans} and v_p values being close to the median for the group. It can be seen that, while the vascular input functions are very similar (Figure S1A), the tissue curves begin to diverge, particularly for the PD group (Figure S1B). Baseline T_1 values did not vary significantly between the groups, with mean \pm SE values of CN: 1.70 s \pm 0.04 s, CP: 1.76 s \pm 0.04 s, PD: 1.74 s \pm 0.04 s.

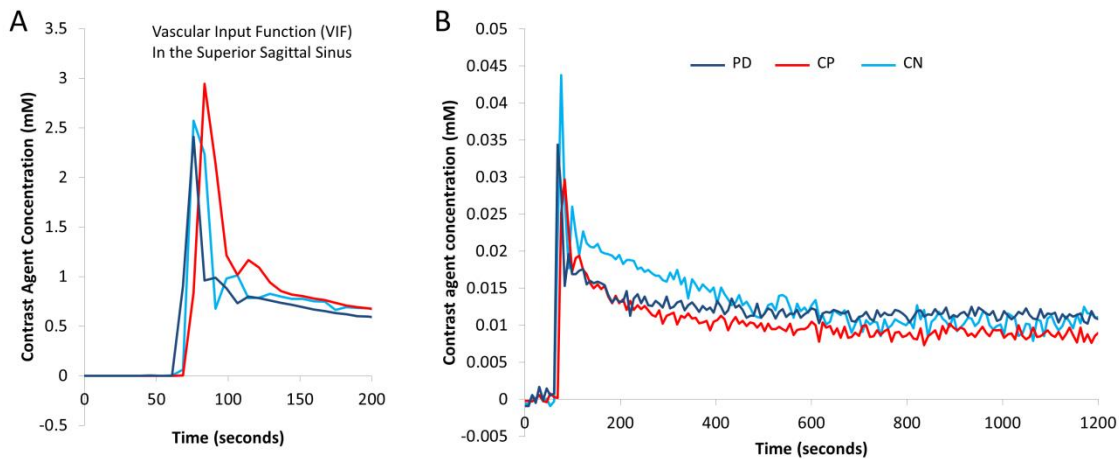


Figure S1: Concentration time-course of contrast agent in blood and tissue

Typical time-courses of the vascular input function (A) and the white matter contrast agent concentration (B) taken from representative subjects of each group. Subjects were selected according to K^{trans} and v_p values being close to the median for the group.

2. Results

2.1 Voxel-wise analysis

Tables S1, S2, S3, S4 and S5 provide details of the regions showing group differences in the voxel-wise analysis, highlighting regions of significant difference in K^{trans} between the PD and CN groups (Table S1), the PD and CP groups (Table S2) and the CP and CN groups (Table S3) and regional differences in v_p between the CP and CN groups (Table S4) and CP and PD groups (Table S5).

Table S1. Regions of significantly higher K^{trans} in the PD group than in the CN group. The t-values are thresholded with voxel-level $p < 0.001$ (uncorrected) and minimum cluster size of 50 voxels.

Region	Cluster size	Cluster p (FWE corr)	Peak t-value	Peak p (uncorr.)	Peak MNI coordinates
White matter in the R hemisphere precuneus extending into parietal lobe and calcarine	406	0.04	3.96 3.87 3.48 3.36 3.35	<0.0001 0.0001 0.0004 0.0006 0.0006	22 -56 32 32 -40 22 28 -36 28 16 -50 10 12 -32 30
White matter in the L and R precuneus extending into paracentral lobule	306	0.1	3.86 3.73 3.60 3.54 3.38	0.0001 0.0002 0.0003 0.0003 0.0006	-6 -40 64 12 -36 60 8 -36 66 -12 -28 52 -12 -38 60
R inf temporal gyrus	82	0.7	3.7	0.0001	50 -26 -26

Table S2. Regions of significantly higher K^{trans} in the PD group than in the CP group. The t-values are thresholded with voxel-level $p < 0.001$ (uncorrected) and minimum cluster size of 50 voxels.

Region	Cluster size	Cluster p (FWE corr)	Peak t-value	Peak p (uncorr.)	Peak MNI coordinates
White matter in R temporal lobe	69	0.8	3.73	0.0002	34 -60 16

Table S3. Regions of significantly higher K^{trans} in the CP group than in the CN group. The t-values are thresholded with voxel-level $p < 0.001$ (uncorrected) and minimum cluster size of 50 voxels.

Region	Cluster size	Cluster p (FWE corr)	Peak t-value	Peak p (uncorr.)	Peak MNI coordinates
R cerebellum	233	0.1	3.96 3.85	0.0001 0.0002	34 -80 -30 20 -82 -24
Midline cingulate gyrus	104	0.6	3.99 3.79	0.0001 0.0002	0 -24 28 0 -16 32

Table S4. Regions of significantly lower v_p in the CP group than in the CN group. The t-values are thresholded with voxel-level $p < 0.001$ (uncorrected) and minimum cluster size of 50 voxels.

Region	Cluster size	Cluster p (FWE corr)	Peak t-value	Peak p (uncorr.)	Peak MNI coordinates
White matter of L temporal lobe	242	0.3	4.46 4.04 3.76	<0.0001 0.0001 0.0003	-36 -40 4 -32 -54 6 -22 -68 8
White matter of R temporal lobe extending into insula and sup. temporal gyrus	290	0.2	4.34 4.16 4.12 3.92	<0.0001 <0.0001 <0.0001 0.0002	38 -34 0 40 -22 -4 38 -26 -2 42 -22 4
L sup. temporal gyrus	53	0.8	3.80	0.0002	-40 -60 26

Table S5. Regions of significantly lower v_p in the CP group than in the PD group. The t-values are thresholded with voxel-level $p < 0.001$ (uncorrected) and minimum cluster size of 50 voxels.

Region	Cluster size	Cluster p (FWE corr)	Peak t-value	Peak p (uncorr.)	Peak MNI coordinates
White matter of the R temporal lobe	65	0.8	4.00	<0.0001	40 -34 -4
White matter of the L temporal lobe	85	0.7	3.93 3.67	0.0001 0.0003	-36 -40 0 -34 -46 4

2.2 ROI analysis with scanner and gender matching

To check that any apparent group differences in imaging metrics were not driven by group differences in gender or scanner used, we repeated the ROI analysis on a selected group of participants with these factors matched across groups.

2.21 ROI analysis with scanner matching

Table S6 demonstrates the demographics for participants whose data was collected on the same scanner at the Manchester Clinical Research Facility. Figure S2 shows regional values for K^{trans} and v_p using data collected from these groups. The results are in broad agreement with the results reported in the main paper (Figure 4). ANOVA with K^{trans} as the dependent variable and WML volume, age and gender included as covariates showed a significant effect of group ($F = 3.5$, $p=0.04$) and region ($F = 44.6$, $p<0.0001$) on K^{trans} and no significant effect of WML volume ($F=0.4$, $p=0.5$), age ($F=0.4$, $p=0.5$) or gender ($F=0.001$, $p=1.0$). Post-hoc tests again showed K^{trans} to be significantly higher in PD than in CN ($p=0.03$, Bonferroni corrected) and no significant differences between the other two pairwise comparisons. Similar analysis with v_p as the dependent variable showed a significant effect of region ($F =$

55.2, $p < 0.0001$) but not group ($F = 0.9$, $p = 0.4$) on v_p and no significant effect of WML volume ($F = 0.02$, $p = 0.9$), age ($F = 1.6$, $p = 0.2$) or gender ($F = 0.05$, $p = 0.8$).

Table S6: Demographics and clinical and radiological characteristics of the participants for data collected only on the same scanner

	CN (n=20)	CP (n=15)	PD (n=36)	p value PD v CN	p value PD v CP	p value CP v CN
n (F:M)	13:7	4:11	12:37	0.002	0.26	0.02
Age (years): mean (range)	67.8 (51-81)	69.1 (53-84)	70 (52-85)	0.31	0.69	0.64
No. of cardiovascular risk factors: mean (SD)	1.71 (1.31)	2.93 (1.16)	1.72 (1.52)	0.92	0.009	0.006
Cardiovascular Risk Factors (% of group):						
Hypertension	35.0	73.3	38.9	0.22	0.02	0.02
Diabetes mellitus	5.0	13.3	8.3	0.39	0.43	0.50
FH of CVD	50.0	46.7	36.1	0.13	0.19	0.26
Smoker	25.0	66.7	38.9	0.14	0.05	0.01
Hypercholesterolaemia	45.0	68.9	36.1	0.18	0.01	0.07
Ischaemic heart disease	10.0	13.3	16.7	0.26	0.32	0.38
Atrial fibrillation	0	20.0	0	1	0.02	0.07
Disease Duration (years): mean (SD)	N/A	1.1 (0.77)	6.9 (4.38)	N/A	N/A	N/A
Hoehn & Yahr Score: mean (SD)	N/A	N/A	2.61 (0.95)	N/A	N/A	N/A
UPDRS Score: mean (SD)	N/A	N/A	30.4 (11.6)	N/A	N/A	N/A
LEDD (mg): mean (SD)	N/A	N/A	577.5 (329.2)	N/A	N/A	N/A
MoCA Score: mean (SD)	27.7 (2.0)	26.1 (2.9)	24.9 (4.1)	0.001	0.22	0.08
Cube-root of WML volume (mm): mean (SD)	1.37 (0.93)	2.11 (0.72)	2.08 (0.91)	0.009	0.89	0.01

CN: control negative; CP: control positive; FH of CVD: family history of cardiovascular disease; LEDD: levodopa equivalent daily dose; MoCA: Montreal Cognitive Assessment; PD: Parkinson's disease; UPDRS 111: unified Parkinson's disease rating scale motor score; WML: white matter lesion.

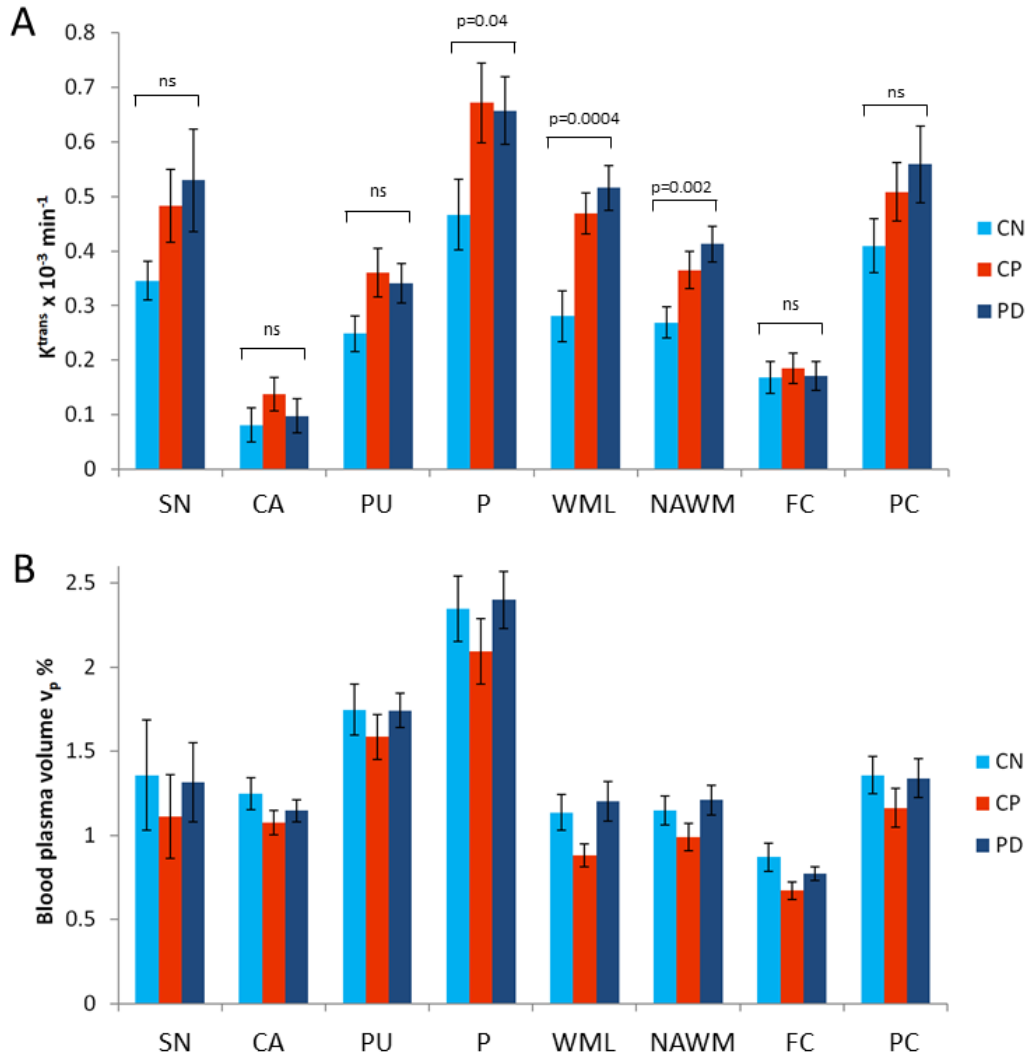


Figure S2: Mean group values for K^{trans} and v_p in regions of interest from data collected on the same scanner

Mean values are given for the (A) the contrast agent transfer coefficient K^{trans} and (B) the plasma volume v_p . Error bars show the standard error in the mean. SN = substantia nigra, CA= caudate, PU = putamen, P = pallidum, WML = white matter lesions, NAWM = normal-appearing white matter, FC = frontal cortex, PC = posterior cortices.

2.22 ROI analysis with gender matching

Table S7 shows the demographics and clinical characteristics of the gender matched groups. Figure S3 show regional values for K^{trans} and v_p using data from these groups. The results are in broad agreement with the results reported in the main paper (Figure 4). ANOVA with K^{trans} as the dependent variable and WML volume, age and gender included as covariates showed a significant effect of group ($F = 3.0$, $p=0.05$) and region ($F = 51.1$, $p<0.0001$) on K^{trans} and no significant effect of WML volume ($F=0.04$, $p=0.8$), age ($F=2.2$, $p=0.14$) or gender ($F=0.1$, $p=0.7$). Post-hoc tests again showed K^{trans} to be significantly higher in PD than in CN ($p=0.04$, Bonferroni corrected) and no significant differences between the other two pairwise comparisons. Similar analysis with v_p as the dependent variable showed a significant effect of region ($F = 88.1$, $p<0.0001$) but not group ($F = 0.8$, $p=0.5$) on v_p and no significant effect of WML volume ($F=0.01$, $p=0.9$), age ($F=1.0$, $p=0.3$) or gender ($F=0.5$, $p=0.5$).

Table S7: Demographics and clinical and radiological characteristics of the gender matched study group

	CN (n=21)	CP (n=15)	PD (n=49)	p value PD v CN	p value PD v CP	p value CP v CN
n (F:M)	6:15	4:11	12:37	0.20	0.25	0.29
Age (years): mean (range)	67.1 (52-81)	69.1 (53-84)	68.9 (52-85)	0.42	0.84	0.44
No. of cardiovascular risk factors: mean (SD)	1.71 (1.31)	2.93 (1.16)	1.72 (1.52)	0.97	0.002	0.003
Cardiovascular Risk Factors (% of group):						
Hypertension	33.3	73.3	26.5	0.20	0.02	0.02
Diabetes mellitus	9.5	13.3	6.1	0.32	0.43	0.44
FH of CVD	52.4	46.7	22.4	0.06	0.15	0.25
Smoker	23.8	66.7	28.6	0.13	0.03	0.01
Hypercholesterolaemia	38.1	68.9	22.4	0.13	0.004	0.05
Ischaemic heart disease	9.52	13.3	12.2	0.24	0.31	0.37
Atrial fibrillation	0	20.0	2.0	0.7	0.04	0.06
Disease Duration (years): mean (SD)	N/A	1.1 (0.77)	7.2 (4.45)	N/A	N/A	N/A
Hoehn & Yahr Score: mean (SD)	N/A	N/A	2.60 (0.09)	N/A	N/A	N/A
UPDRS Score: mean (SD)	N/A	N/A	29.2 (12.7)	N/A	N/A	N/A
LEDD (mg): mean (SD)	N/A	N/A	583.5 (399.6)	N/A	N/A	N/A
MoCA Score: mean (SD)	27.7 (2.4)	26.1 (2.9)	25.3 (3.9)	0.004	0.39	0.10
Cube-root of WML volume (mm): mean (SD)	1.26 (0.81)	2.11 (0.72)	1.80 (0.95)	0.02	0.19	0.002

CN: control negative; CP: control positive; FH of CVD: family history of cardiovascular disease; LEDD: levodopa equivalent daily dose; MoCA: Montreal Cognitive Assessment; PD: Parkinson's disease; UPDRS 111: unified Parkinson's disease rating scale motor score; WML: white matter lesion

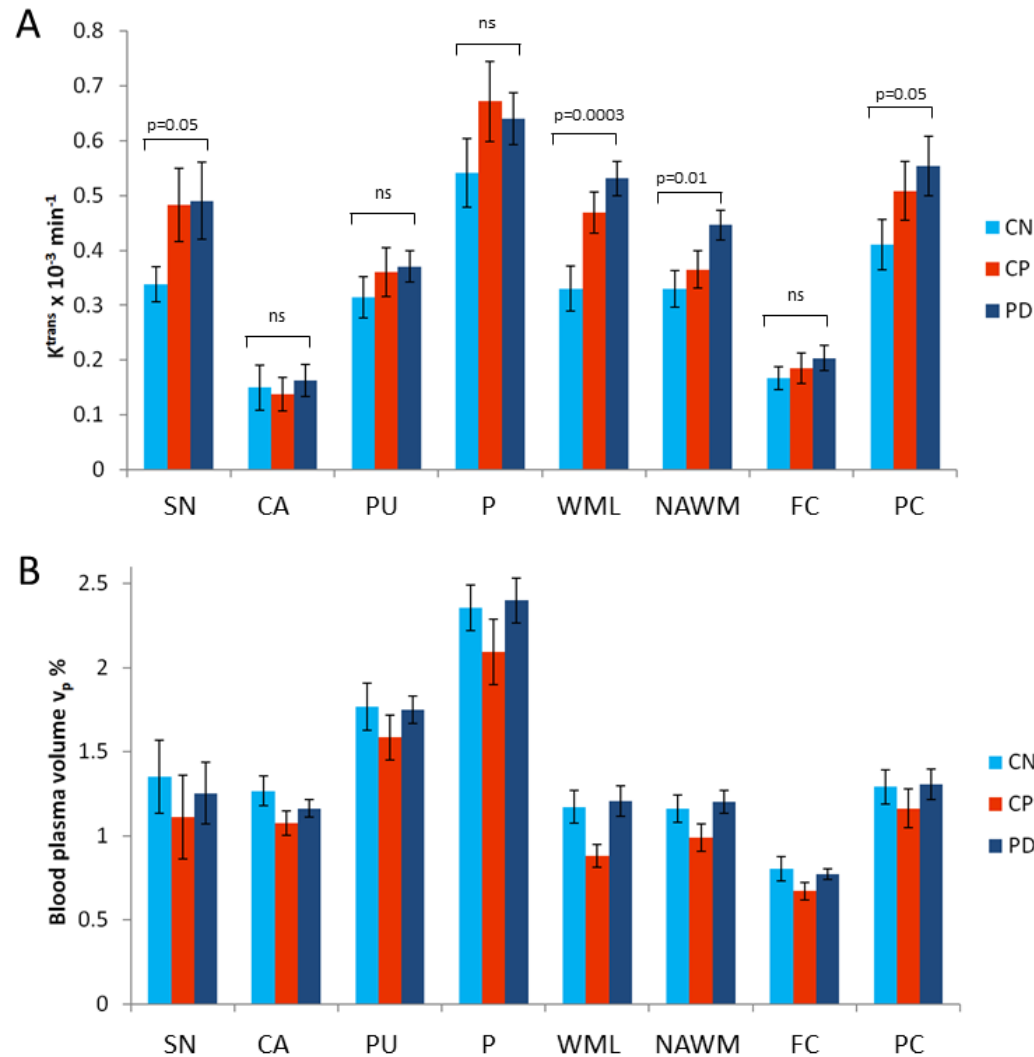


Figure S3: Mean group values for K^{trans} and v_p in regions of interest with matched gender balance between groups

Mean values are given for the (A) the contrast agent transfer coefficient K^{trans} and (B) the plasma volume v_p . Error bars show the standard error in the mean. SN = substantia nigra, CA= caudate, PU = putamen, P = pallidum, WML = white matter lesions, NAWM = normal-appearing white matter, FC = frontal cortex, PC = posterior cortices.

References

1. Fram EK, Herfkens RJ, Johnson GA, Glover GH, Karis JP, Shimakawa A, et al. Rapid calculation of T1 using variable flip angle gradient refocused imaging. *Magn Reson Imaging*. 1987;5(3):201-8.
2. Voigt T, Nehrke K, Doessel O, Katscher U. T1 corrected B1 mapping using multi-TR gradient echo sequences. *Magn Reson Med*. 2010;64(3):725-33.
3. Pohmann R, Scheffler K. A theoretical and experimental comparison of different techniques for B(1) mapping at very high fields. *NMR Biomed*. 2013;26(3):265-75.
4. Cirillo M, Laurenzi M, Trevisan M, Stamler J. Hematocrit, blood pressure, and hypertension. The Gubbio Population Study. *Hypertension*. 1992;20(3):319-26.